Proceedings of the ASME 2021 40th International
Conference on Ocean, Offshore and Arctic Engineering
OMAE2021
June 21-30, 2021, Virtual, Online

OMAE2021-62012

A NUMERICAL STUDY OF THE HYDRODYNAMICS OF AN OFFSHORE FISH FARM USING REEF3D

Gang Wang*
College of Fisheries, Ocean University of China
266003 Qingdao, China
Department of Civil and Environmental Engineering
Norwegian University of Science and Technology
7491 Trondheim, Norway

Tobias Martin
Department of Civil and Environmental Engineering
Norwegian University of Science and Technology
7491 Trondheim, Norway

Liuyi Huang
College of Fisheries, Ocean University of China
266003 Qingdao, China

Hans Bihs
Department of Civil and Environmental Engineering
Norwegian University of Science and Technology
7491 Trondheim, Norway

ABSTRACT

In this paper, the CFD framework REEF3D is utilized to investigate the hydrodynamics of a large offshore fish farm in waves. The solver consists of a rigid body dynamics solver for the frame structure coupled to a fluid solver including the shielding effects of the nets. The solver and the grid independence are validated using a 2D numerical wave tank, a free decay test, and a study of the wave loads on a rigid net panel. Then, the effects of regular wave parameters, the thickness of the vertical outer columns of the structure, and varies aspect ratios on the loads, response and maximum mooring tensions are investigated. It is concluded that the response is sensitive to the wave period rather than the wave height and that the net system accounts for about 30% *of the total drag but does not influence the structural response to a larger extend. The effect of the aspect ratio on the hydrodynamics is more distinct than that of the frame thickness especially. Thus, the first step towards a systemic evaluation of the importance of different structural parts of an offshore fish cage for the expected responses is presented in this paper.*

Keywords: *Fluid-structure interaction, Offshore fish farm, Hydrodynamics, CFD*

1 INTRODUCTION

In recent time, a tendency of moving aquaculture sites towards the open ocean area is observable due to the restrictions of space and ecology in near shore regions and despite the risks connected to complex sea states. As a promising solution, the development of open ocean aquaculture (OOA) farms, including semi-submersible and submerged rigid structures, has been initiated lately. The most popular OOA structures are the circular fish farms “Ocean Farm 1” in Norway, “ShenLan 1” in China and the prospective “ShenLan 2” as well as the vessel-shaped farms “HavFarm 2” and “Dehai 1”. The appearance of these new type of structures requires new as well as comparative studies of the correlations between hydrodynamic characteristics and structural features. Consequently, the accurate knowledge of the hydrodynamic responses is key for the optimal design of OOA facilities. A distinctive difference between OOA and traditional offshore structures lies in net systems which are exposed to the hydrody-

*Corresponding author: gang.wang@ntnu.no; wg@stu.ouc.edu.cn

namic loads while also risking the collision with fishes which might lead to the damage of the net. Even though the linear potential theory can be applied to simple floating bodies, more advanced hydrodynamic tools are required to evaluate the risks of OOA structures in severe environments while also including two-way coupling to the net and the mooring system.

The hydrodynamic characteristics of OOA structures in waves were investigated using numerical simulations relying on linear potential theory, Computational Fluid Dynamics (CFD), and physical experiments. The numerical study of a vessel-shaped fish farm was presented in [1] and [2] using a screen force model for the hydrodynamics of the nets and linear potential theory for the rigid body motions, mooring system and waves. However, no validation was presented. An experimental investigation of a circular OOA structure in waves was performed in [3]. A numerical study of these measurements was performed in [4] using a boundary element method. Here, the authors adopted a Morison force model for the hydrodynamics on nets and the structure which disregards the non-linear interaction. Moreover, the hydrodynamics of a single point moored semi-submersible vessel-type OOA structure has been evaluated in [5]. All the mentioned studies neglect the non-linear wave-structure interaction which prevents gaining more insights about the hydrodynamic characteristics of OOA structures, especially in severe offshore scenarios. The first model suitable for these applications was given in [6] using a novel continuous direct forcing approach for incorporating three-dimensional floating bodies coupled with a net solver [7] and the shielding effects of the net on the fluid [8] in a CFD approach. Hence, the fluid-structure interaction as well as non-linear effects of the waves could be investigated in a two-way coupled manner.

In this paper, the model in [6], implemented in REEF3D [9, 10], is utilised to investigate the effects of structural features and different wave conditions on the hydrodynamics of a OOA structure. The largest offshore fish farm "ShenLan 1" is taken as application as it represents a typical circular OOA structure. The effects of regular wave parameters, the thickness of the vertical columns and the aspect ratio of the farm on the response, wave loads and maximum mooring tensions are discussed. Additional validation cases of a 2D numerical wave tank (NWT), a free-decay test, and a rigid net panel are presented to ensure the accurate wave propagation and grid independence. Hence, the structure of the remaining paper is as follows: Section 2.1 introduces the numerical model. Sections 2.2 describes the prototype model and the numerical setup. Afterwards, the validation cases are presented in Section 3, and the study of the OOA structure follows in Section 4). Finally, Section 5 gives final remarks.

2 MATERIAL AND METHODS

2.1 Numerical model

The conservation of mass and momentum of an incompressible fluid is described through the three-dimensional continuity and Reynolds-averaged Navier-Stokes (RANS) equations

$$\begin{aligned} \frac{\partial u_i}{\partial x_i} &= 0, \\ \frac{\partial u_i}{\partial t} + u_j \frac{\partial u_i}{\partial x_j} &= -\frac{1}{\rho}\frac{\partial p}{\partial x_i} + \frac{\partial}{\partial x_j}\left[(\nu+\nu_t)\left(\frac{\partial u_i}{\partial x_j}+\frac{\partial u_j}{\partial x_i}\right)\right] + g_i, \end{aligned} \quad (1)$$

where u_i represents the velocity vector, ρ is the fluid density, p is the pressure, g_i is the gravity acceleration vector and ν and ν_t denote the kinematic and eddy viscosity in the diffusion term. The free surface is implicitly captured as the interface of the two phases air and water represented by the zero level set of the smooth signed distance function Φ [11]. An advection equation is formulated for Φ to propagate it in space and time:

$$\frac{\partial \Phi}{\partial t} + u_j \frac{\partial \Phi}{\partial x_j} = 0. \quad (2)$$

A reinitialization procedure is introduced to keep the signed distance property of Φ after each time step. The density and viscosity are calculated in the two phases as

$$\begin{aligned} \rho &= \rho_w H(\Phi) + \rho_a (1 - H(\Phi)), \\ \nu &= \nu_w H(\Phi) + \nu_a (1 - H(\Phi)), \end{aligned} \quad (3)$$

where w indicates water, a stands for air and $H(\Phi)$ denotes the smoothed Heaviside step function [10]. The generation of the waves is achieved by prescribing the wave velocities and free surface elevation at the inlet boundary [12]. Besides, the waves are damped at the end of the domain using a numerical beach as presented in [13]. The system of equations is solved using finite differences on a rectilinear, staggered grid. Fifth-order accurate weighted essentially non-oscillatory (WENO) schemes [14, 15] are applied for the spatial discretization of convection terms. The diffusion terms are discretized with a second-order central difference scheme. The explicit third-order accurate TVD Runge-Kutta method [16] is utilized for the time discretisation. The coupling between velocity and pressure in Eq. 1 is ensured using the projection method as described in [6].

Rigid floating bodies are incorporated in the solver using an additional signed distance field Φ_s to distinguish between fluid and solid phase. The boundary conditions between the two phases are implicitly incorporated in the momentum equations using a direct forcing approach. Here, the source term

$$f = H(\Phi_s) \cdot \left(\frac{\mathbf{P}(u)\text{-}u}{\Delta t}\right) \quad (4)$$

is added to the equations before the projection step. In (4), P(u) represents the divergence free rigid body velocity field which can be calculated from solving Newton's second law for the structure (see [6] for details). The forces and moments acting on the floating body are calculated based on the integration over the triangulated body surface with N triangles:

$$F_x = \sum_{i=1}^{N} (-\mathbf{n}p + \rho\nu\mathbf{n}\tau)_i \cdot \Delta\Omega_i,$$
$$M_x = \sum_{i=1}^{N} \mathbf{r}_i \times (-\mathbf{n}p + \rho\nu\mathbf{n}\tau)_i \cdot \Delta\Omega_i. \quad (5)$$

Here, $\mathbf{n}$ is the surface normal vector, τ is the stress tensor and $\mathbf{r}$ denotes the distance vector from each element to the centre of gravity.

The nets are assumed to be rigid due to their high stiffness. Therefore, the forces on the net are added to the floating body solver as external forces. These are particularly the hydrodynamic drag and lift forces. As explained in [8], the forces cannot be calculated by directly integrating over the structural surface of the nets because of the computational costs. Instead, a screen force model is utilised to approximate the hydrodynamic loads from the fluid solution:

$$F_i = \sum_{s=1}^{E_s} \frac{\rho}{2} A_s u_{rel,s}^2 (c_d \boldsymbol{n}_d + c_l \boldsymbol{n}_l)_s,$$
$$c_d(\alpha) = c_{d,0} \sum_{k=1}^{\infty} a_{2k-1} \cos((2k-1)\alpha),$$
$$c_l(\alpha) = c_{l,\frac{\pi}{4}} \sum_{k=1}^{\infty} b_{2k} \cos(2k\alpha), \quad (6)$$

with $\boldsymbol{n}_d$ the normal and $\boldsymbol{n}_l$ the tangential direction of the relative velocity vector $\boldsymbol{u}_{rel,s}$. The constants $c_{d,0}$ and $c_{l,\frac{\pi}{4}}$ are taken from [17], and the Fourier coefficients are fitted non-linearly using experimental data. Two-way coupling is enabled by including the momentum loss of the fluid through the net as a source term in the momentum equation. Hence, the correct velocity reduction behind the nets can be approximated. The source term S is obtained at each fluid grid point from the surrounding net surface using the hydrodynamic loads from the screen force model (see [7] for details).

2.2 "ShenLan 1" offshore fish farm and numerical setup

The "ShenLan 1" offshore fish farm is the largest OOA structure in China. It is placed in the cold water region of the Yellow Sea which can be subject to extreme sea states in the open ocean areas. Equipped with two cylindrical liquid-gas tanks, the draught of the structure can be adjusted in order to vary the water temperature for the fish inside. The frame contains a rigid frame composed of 8 vertical columns, a four-point mooring system consisting of pre-tensioned chains, and a Ultra-High-Strength-Polyethylene square nets system with twine diameters of 3.0 mm and twine lengths of 2 cm. The operation site is about 130 miles off the coast, and the practical working state corresponds to 30 m-draught. The full-scale diameter, referring to the distance between the opposite farthest vertical columns, is 60.44 m, and the full-scale height of the cage is 34.45 m. The steel frame (Fig. 1b) is the main component to resist severe environmental loads and conserve the cage volume.

(a)

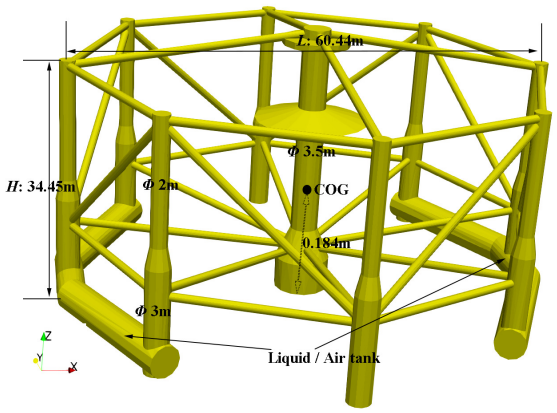

(b)

FIGURE 1. "SHENLAN 1" OFFSHORE FISH FARM, (C) THE MODELLED FRAME SYSTEM.

In this study, a 1:60 model scale based on Froude scaling is

investigated. As explained in [3], a uniform scaling ratio is not applicable to the nets of offshore fish farms since the dimension of the net twines is already in full-scale extremely small. Therefore, the diameter and length of the bars of the rigid net are not scaled. Following the analysis in [3], the mooring lines are modelled as linear springs with pre-tension and stiffness calculated using elastic similarity. Tab. 1 summarises the structural dimensions and system parameter in the chosen model scale.

TABLE 1. Main structural data of the model-scaled "ShenLan 1" fish farm in the working state.

Parts	Item	Data [m]
Peripheric diameter	-	1.007
Peripheric height	-	0.574
Central pipe	Length	0.577
	Diameter	0.058
Outer pipe	Length	0.251 (Upper parts)
		0.215 (Lower parts)
	Diameter	0.033 (Upper parts)
		0.050 (Lower parts)
Thin pipe	Diameter	0.017
Nets	Bar length	0.02
	Bar diameter	0.003
	Solidity ratio	27.75%
Mooring	Stiffness	187 N/m
	Pre-tension	1.9 N
Weight	-	15.9 Kg

The floating model is placed in a 3D NWT with the dimensions 7.23 m × 1.6 m × 1.5 m (Fig. 2). The length of the domain is determined by the mooring positions and the accurate wave transmission with minimum wave damping as discussed in section 3. The waves are generated at the inlet using the Dirichlet method, and the relaxation method is utilized to absorb the waves in a numerical beach at the end of the tank. Symmetry conditions are assigned on the side walls and the top of the tank, while the bottom is treated with non-slip wall boundary conditions. The waves are modelled as regular 2nd-order Stokes waves with the wave heights H=0.04 m, 0.12 m, 0.20 m and wave periods T=0.8 s, 1.0 s, 1.2 s, 1.4 s.

3 VALIDATIONS

At first, the accuracy of the wave propagation is validated using a 2D NWT without a structure (Fig. 3). The 2nd-order Stokes wave with H=0.04 m and T=0.5 s is generated, and the wave elevation

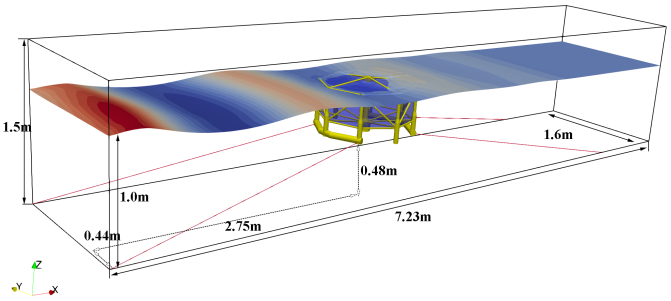

FIGURE 2. THE COMPUTATIONAL DOMAIN.

is measured two wave lengths behind the inlet (WG1). A comparison to the theoretical values is presented in Fig. 4. The phase shift is observed for the coarsest grid with dx=0.012 m. But, the phase converges towards the correct results with decreasing cell size. The amplitudes are close the theoretical values with deviations less than 5% at all time.

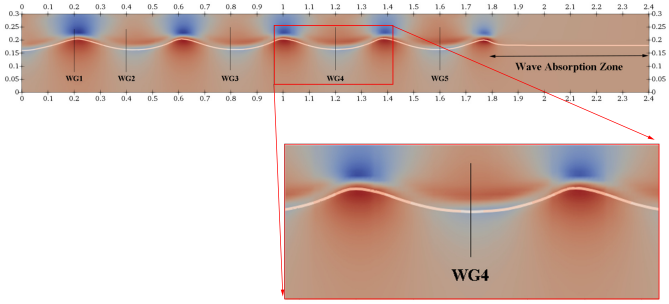

FIGURE 3. SKETCH OF THE 2D NUMERICAL WAVE TANK WITH ABSORPTION ZONES. THE CONTOUR SHOWS THE HORIZONTAL VELOCITY COMPONENT, AND THE SOLID LINES INDICATE THE WAVE GAUGES SET-UP.

Next, the accuracy of the solver for the rigid body motion is validated using the free heave decay test of a cylindrical floater. The correct motion of cylindrical floaters is essential for the accurate prediction of the motion of complete aquaculture plants [18] as it represents the fundamental component of circular OOA structures like "ShenLan 1". The cylinder has a height of 0.355 m, a diameter of 0.050 m and a mass of 0.601 kg. The initial displacement of the buoy is 40 mm below the water level. The heave motion from this position is simulated using REEF3D and compared to the measurement in [19] (see Fig. 5). For all chosen grid sizes, the simulated heave motion follows the measured results properly. On the coarsest grid, numerical diffusion results in over-prediction of the second peak. The finer grids converge

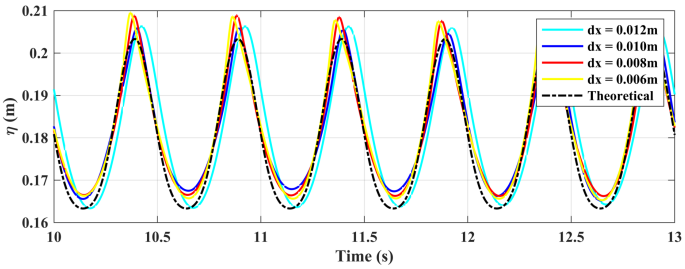

FIGURE 4. GRID INDEPENDENCE TEST AND WAVE PROPAGATION AT WG1 IN A 2D NWT.

well towards the experimental results. Therefore, it is decided to use dx=0.008 m and more refined grids for the subsequent studies.

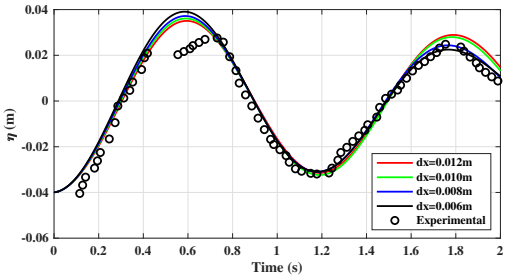

FIGURE 5. GRID INDEPENDENCE TEST AND FREE DECAY TEST OF A CYLINDRICAL BUOY.

Finally, the hydrodynamic loads on a net panel in regular waves are compared to experiments for validation purposes. The measurements of the wave loads on a 50 cm × 50 cm knotless polyethylene net panel in [20] is used for this purpose. The experimental setup is replicated in a numerical wave tank of 10 m × 1.5 m × 4.0 m. The rigid panel is placed perpendicular to the wave propagating direction in the centre of the tank. The twine diameter and the twine length are 2.12 mm and 16.24 mm, respectively. The time signal of the horizontal wave loads on the net are compared to the experimental results in Fig. 6. The frequency of the force signal is captured accurately by the numerical model. Further, the model tends to over-predict the crests by up to 18%. The force troughs agree better with the experiments in some time instances. Overall, the results are agreeable and coincide with previous studies of this model [8].

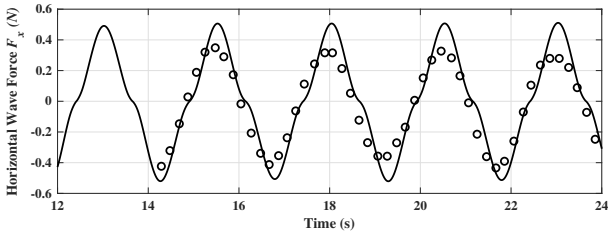

FIGURE 6. COMPARISONS BETWEEN SIMULATED (SOLID LINE) AND MEASURED ("O" SYMBOLS) HORIZONTAL WAVE FORCES ON NET PANELS.

4 RESULTS AND DISCUSSIONS

In the following, the effects of varying wave parameters, column diameters, and aspect ratios between diameter and height of the overall structure on the hydrodynamics are discussed. Here, the linear transfer functions of the motions in terms of Response Amplitude Operators (RAO), the maximum mooring line tensions and the hydrodynamic wave loads on the OOA structure including nets are utilised for an analysis in time and frequency domain. The RAO is calculated using the power spectra obtained from an FFT analysis of the wave and motion signals:

$$RAO = \sqrt{\frac{S_{motion}}{S_{wave}}}. \tag{7}$$

Here, S_{motion} and S_{wave} represent the power spectra from the auto-correlation analyses.

4.1 Effects of wave parameters on the hydrodynamics

The variation of the RAO for heave, surge, and pitch due to the different wave periods and wave heights for "ShenLan 1" are illustrated in Fig. 7. For the cases with varying wave periods, the wave height is 0.12 m, and for the wave height cases, the wave period remains at 1.0 s. It can be observed that the heave, surge, and pitch RAO show a non-linear increase for increasing wave periods, which is in accordance with the observations in [4]. It is shown that the response of a high-damped floating system, such as given in this case, to high-frequency wave excitations is generally small [21]. Further, the simulations in varying wave heights reveal less variation, especially for the surge motion, and the amplitudes of the heave and surge motions rise sharply with increasing wavelengths for cases with similar wave steepnesses (e.g. H=0.12 m, T=1.4 s; H=0.04 m, T=1.0 s). This might be explained by the longer duration of unidirectional wave loads acting on the OOA frame. These scenarios are also shown in the

Figs. 8(a) and (b) for wave crest situations. Moreover, the difference between the largest wavelength case and the case with the maximum wave height is visualised similarly in the Figs. 8(b), (c), and (d). It is interesting to notice that the flume experiments of "Ocean Farm 1" reported in [3] and simulated using CFD in [6] reveal larger surge motions in steeper waves which is the opposite of the results for "ShenLan 1". This difference might be caused by the distinct structural differences between "Ocean Farm 1" and "ShenLan 1" such as the difference of the ratio of height to diameter of the cage. Also, the studied fish farm encounters partial submersion and wave overtopping over the top of side vertical columns in very steep waves (see Fig. 9) which is not observed for "Ocean Farm 1".

A distinction between traditional semi-submersible offshore platforms and OOA fish farms lies in the net system. It is indicated in Fig. 7 that the damping effect of nets on the predicted RAO is rather small except for the three responding motions in shallow waves (H=0.12 m, T=1.4 s; H=0.04 m, T=1.0 s). More investigations are necessary to account for the deviation in this scenario. Similar observations are also given in [3] and [6], and it shows that the translational motions are mainly dominated by the rigid floating frame and the mooring system.

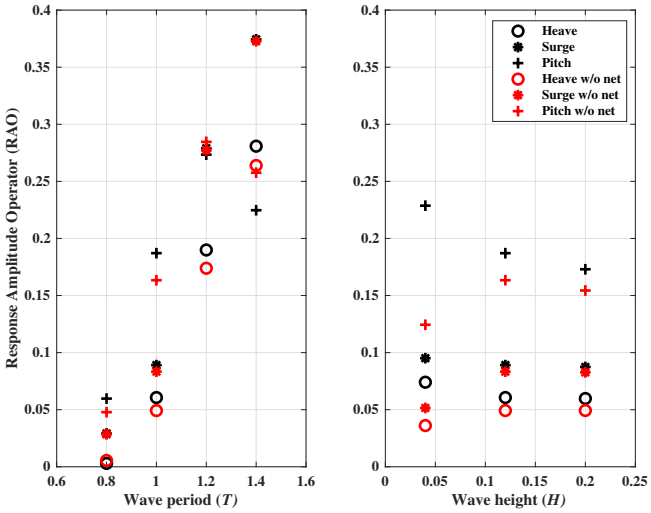

FIGURE 7. RESPONSE AMPLITUDES OF THE "SHENLAN 1" OVER VARIES WAVE PERIODS AND WAVE HEIGHTS.

Next, the horizontal and vertical hydrodynamic loads on the frame and net parts are discussed. The load amplitudes are presented as their main, linear and second harmonic components from an FFT analysis in Fig. 10. It can be seen that the presence of nets affects the hydrodynamic loadings on frame systems

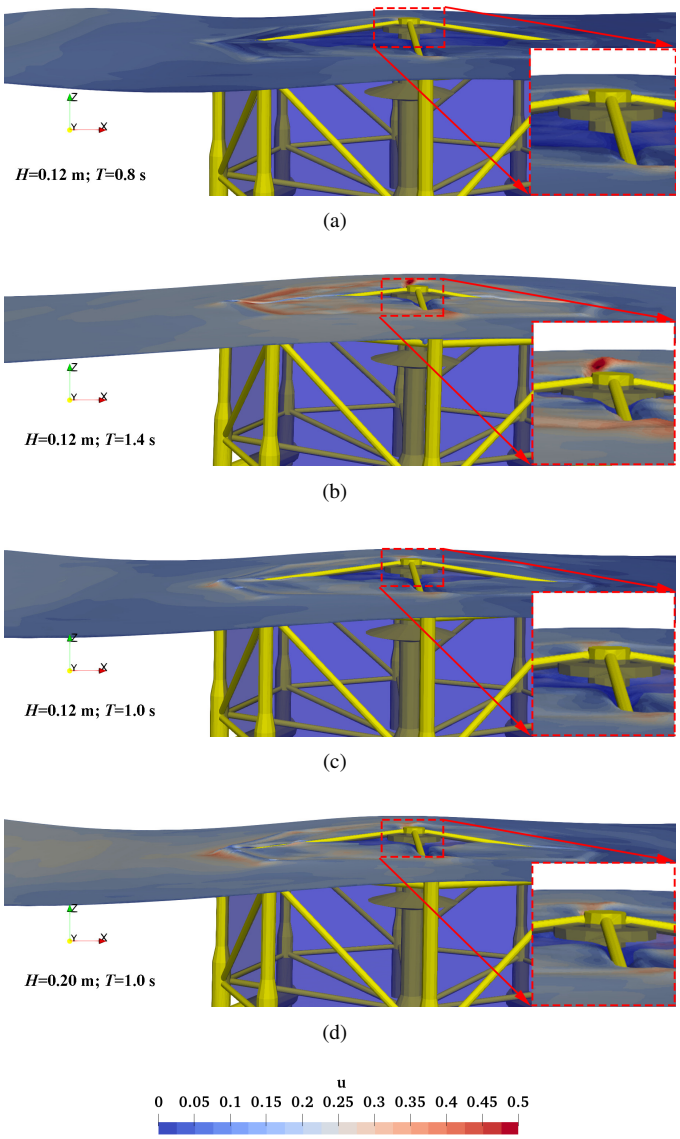

FIGURE 8. THE COMPARISON BETWEEN CASES WITH VARIOUS WAVE PERIODS AND WAVE HEIGHTS AT THE WAVE CREST SCENARIOS.

around approximate 10% varying wavelengths. Further, the linear and higher harmonics of the horizontal force on the frames and nets increase non-linearly if the wave frequency decreases. A possible explanation is that the wave forces surge dramatically when the wavelength exceeds the horizontal dimension of OOA structures [22]. The mean horizontal force component is generally small and oscillates for varying wavelengths. The 2nd-order harmonics exceed the mean component, especially for the net forces. It is to be noticed that this unsteady non-linear force fluctuations can cause the breakage of net twines. Additionally, the horizontal forces on the net account for approximately 30% of

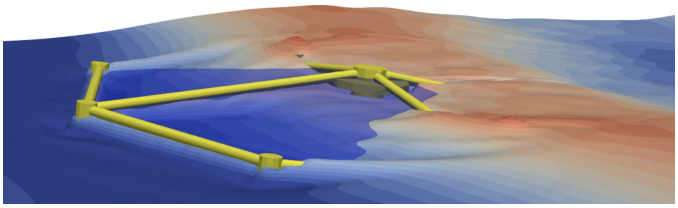

(a)

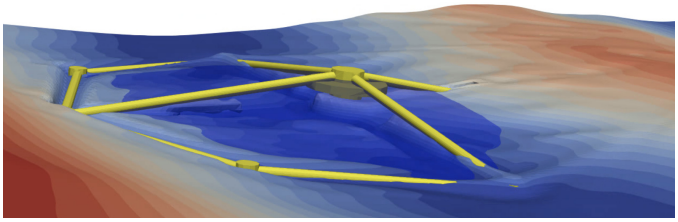

(b)

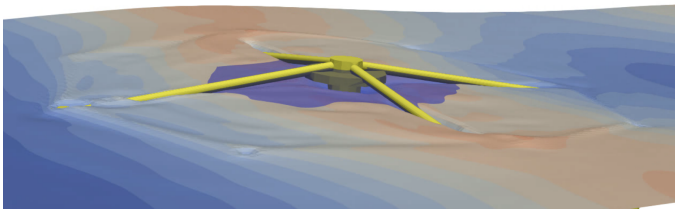

(c)

FIGURE 9. TIME HISTORY OF FREE SURFACE ELEVATION OVER A WAVE PERIOD FOR CASE H=0.2 M, T=1.0 S

the total horizontal forces, which has been reported previously in [6] for a different OOA structure. The increase of wave height results in a non-linear increase of the mean part due to the increased wave energy, whereas the higher-order components increase linearly with a smaller slope. Thus, it can be concluded that a sudden increase of the wave height, such as in extreme sea states, poses a real threat to the frame system of OOA structures.

For the vertical force amplitudes in Fig. 10(b), the loads on the nets are not considered since most nets are attached to side vertical columns. The mean force amplitude increases slightly with the increase of the wave frequency and wave height, i.e. the wave energy, and it is the main component of the total load. The 2nd-order harmonic remains constant across all cases, whereas the linear vertical wave force component increases significantly and exceeds the amplitude of the mean component for wave periods between 1.0 s and 1.4 s. This is similar to the behaviour observed for the horizontal force amplitudes. Also, all harmonics increase synchronously for changing wave heights, but the mean term is generally 5-10 times larger than the linear and 2nd-order terms.

Due to the symmetry of the octagonal OOA structure shown in Fig. 2, a mooring line on the windward side and another on the

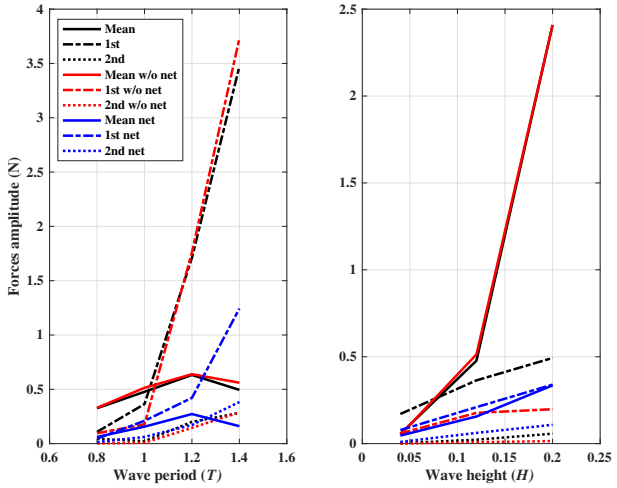

(a) Horizonal wave forces amplitudes

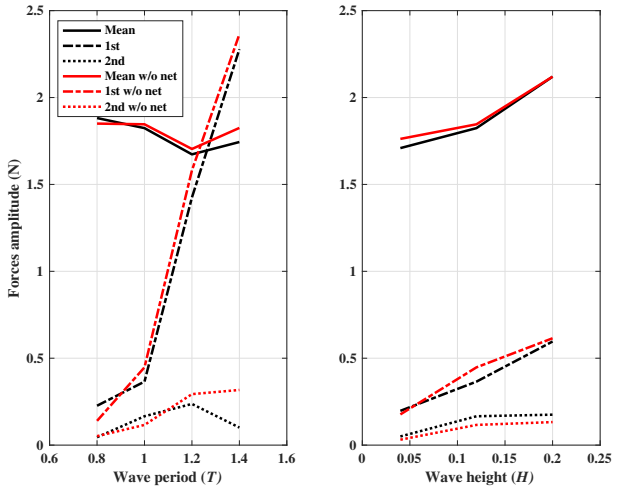

(b) Vertical wave forces amplitudes

FIGURE 10. FOURIER AMPLITUDES OF THE MEAN, FIRST AND 2ND-ORDER HARMONIC COMPONENTS OF THE WAVE FORCES OVER THE WAVE PERIOD AND WAVE HEIGHT. THE BLACK AND RED LINES DENOTE THE WAVE LOADINGS ON FRAME SYSTEMS WITH OR WITHOUT NETS, RESPECTIVELY.

leeward side are chosen to study the maximum tension force amplitudes. It is shown in Fig. 11 that the maximum tension forces are proportional to the wave period as they increase to 3.5 times the tension forces predicted for the lowest wave period case. The forces in the windward mooring line are generally larger than that in the leeward line which was also reported experimentally for "Ocean Farm 1" in [3]. Besides, the effects of the wave period on the windward lines are larger than that of the wave height.

In contrast, the tension forces in the leeward mooring lines increase firstly then decrease considerably with increasing wave heights. It might be caused by the decreasing pitch motions for wave heights ranging from 0.12 m to 0.2 m (compare Fig. 7).

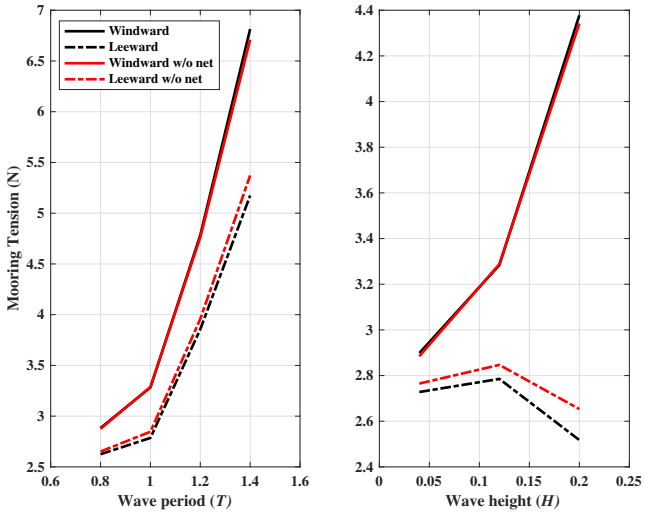

FIGURE 11. MAXIMUM TENSION FORCE AMPLITUDES FOR DIFFERENT WAVE PERIODS AND WAVE HEIGHTS.

4.2 Effects of the diameter of the vertical columns on the hydrodynamics

Fig. 12 presents the RAO, wave forces amplitudes and maximum mooring tension forces for "ShenLan 1" with varying diameter of the vertical outer columns. The diameter is increased and decreased by up to 50% compared to the prototype. The steepest and highest-frequency wave scenario (H=0.2 m and T=1.0 s) is adopted to carry out this study. The total mass and the centre of gravity are adjusted according to the new mass distributions. The effect of the nets is not considered due to its minor influence on the results above. It is first noticed from the results that the translational and rotational motions are independent of the variations of the diameter. Further, the mean components of the loads show a gradual increase in the horizontal direction, whereas the linear and 2nd-order components are less influenced by the diameters. In contrast, the increase of the cylindrical diameters shows a significant effect on the vertical force amplitudes and the maximum mooring line tensions. This is attributed to the combined role of the mass increase induced by the increased diameters and the pre-tension magnitude of the mooring line which are adjusted to the corresponding mass.

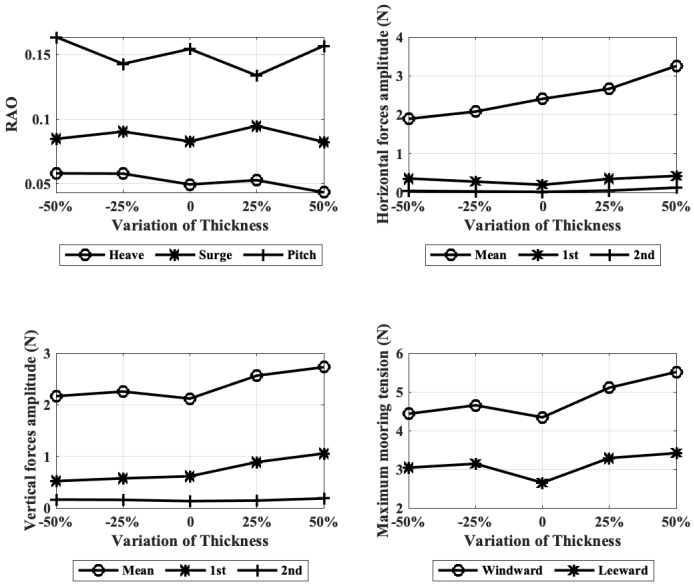

FIGURE 12. HYDRODYNAMICS OF THE OOA FOR VARYING DIAMETER OF THE VERTICAL COLUMNS. THE INDEX "0" DENOTES THE PROTOTYPE.

4.3 Effects of the aspect ratio of OOA structure on the hydrodynamics

A considerable correlation between vibrations with the aspect ratio of floating bodies are clarified in [23]. The aspect ratio of circular OOA structures is defined as L/H (compare Fig. 1(b)) and equals 2.0 for the prototype, it should be noticed that the aspect ratio for Ocean Farm 1 is 2.5 [3]. The RAO, the wave force amplitudes and the maximum mooring tensions of the "ShenLan 1" for aspect ratios up to 2.5 are illustrated in Fig. 13. It is shown that the amplitudes of the heave, surge, and pitch motions decrease with increasing aspect ratios. This is caused by the increased moments of inertia and changing ratio between wave and structural length. It should also be noticed that the results for the aspect ratio of 2.5 are close to the simulations of Ocean Farm 1 for the same wave frequency [6]. Further, the mean component of the horizontal and vertical forces are predicted to gradually increase with the aspect ratio due to the larger area passed by the fluid. In contrast, the linear and 2nd-order force harmonics tend to decrease with increasing aspect ratio because of the reduced motions of the structure. The same argument holds for the observation that the maximum mooring line tensions on the windward and leeward side decrease with the aspect ratio.

5 CONCLUSIONS

In this paper, a numerical study of the hydrodynamics of the open ocean aquaculture fish farm "ShenLan 1" is presented using the

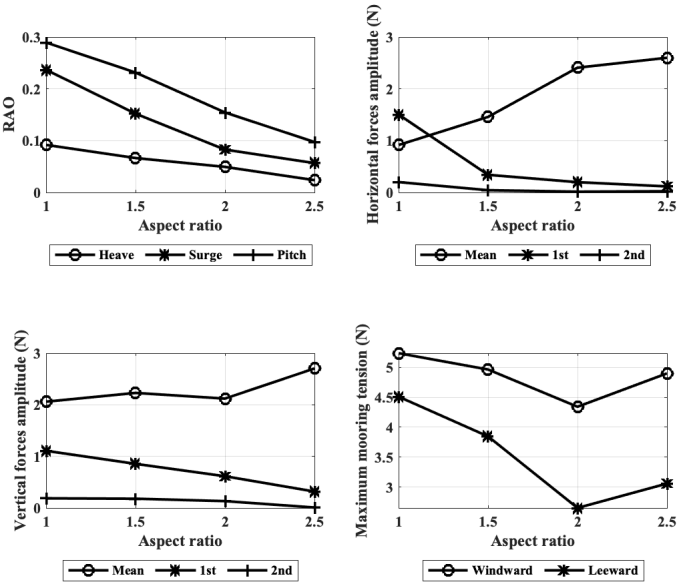

FIGURE 13. HYDRODYNAMIC RESPONSE WITH THE ASPECT RATIO OF THE OOA STRUCTURE.

CFD framework REEF3D. The accuracy of the numerical model is first validated against theoretical and experimental results for wave propagation and a heave decay test for a cylindrical floater. Based on these results, the computational grid and the length of the numerical wave tank were determined. An additional comparison of the hydrodynamic loads on a net panel in regular waves revealed the principal working of the net algorithm implemented in the CFD solver. Then, the response amplitude operator, wave loads and maximum tension forces in the mooring lines are discussed for varying wave parameters and structural parameters. The RAOs of the heave, surge, and pitch motions show non-linear correlations with the wave periods, but the motions are less sensitive to the wave height. It is further shown that the acceleration of the water particles and the exposed area of the structure with the free surface results in strongly oscillatory motions. Further, the wave run-up and partial submersions over the top area of "ShenLan 1" imply increased wave loads. The linear and second-order wave load components on the frame and the net increase with increasing wavelength and height, while the mean component remains constant. The maximum tensions in the windward and leeward mooring lines are dependent on the wave period, wavelength, and the structural motions. In addition, the nets have only minor effects on the translational and rotational motions of the structure even though it accounts for 30% of the total drag on the system. Finally, the effects of changing column diameters and aspect ratios are investigated. It is concluded that the RAOs are not influenced by the investigated range of column diameters, whereas thicker columns lead to larger wave loads and increased mooring tension forces due to the increased area interacting with the fluid. In contrast, the aspect ratio influence reveals a large impact on the motions of the structure. The translational and rotational motions decrease while increasing the aspect ratio to up to 2.5. The mean component of the horizontal and vertical force signal shows an increasing trend with increasing aspect ratios because of the larger exposure area.

ACKNOWLEDGMENT

The authors are grateful for the grants provided by the National Key Research and Development Program of China (Project No. 2019YFD0901000), Research Council of Norway under the HAVBRUK2 project (No. 267981), and the State Foundation for Visiting Ph.D. student from China Scholarship Council (No. 201906330049). The computations were performed on resources provided by UNINETT Sigma2 - the National Infrastructure for High Performance Computing and Data Storage in Norway (`http://www.sigma2.no`) under project No. NN2620K.

REFERENCES

[1] Li, L., Jiang, Z., Høiland, A. V., and Ong, M. C., 2018. "Numerical analysis of a vessel- shaped offshore fish farm". J. Offshore Mech. Arct. Eng., **140**(4), p. 041201.

[2] Li, L., Jiang, Z., Ong, M. C., and Hu, W., 2019. "Design optimization of mooring system: An application to a vessel-shaped offshore fish farm". Eng. Struct., **197**, p. 109363.

[3] Zhao, Y., Guan, C., Bi, C., Liu, H., and Cui, Y., 2019. "Experimental investigations on hydrodynamic responses of a semi-submersible offshore fish farm in waves". J. Mar. Sci. Eng, **7**(238), p. 7070238.

[4] Liu, H.-F., Bi, C.-W., and Zhao, Y.-P., 2020. "Experimental and numerical study of the hydrodynamic characteristics of a semisubmersible aquaculture facility in waves". Ocean Eng., **214**, p. 107714.

[5] Huang, X.-H., Liu, H.-Y., Hu, Y., Yuan, T.-P., Tao, Q.-Y., Wang, S.-M., and Liu, Z.-X., 2020. "Hydrodynamic performance of a semi-submersible offshore fish farm with a single point mooring system in pure waves and current". Aquac Eng, **90**, p. 102075.

[6] Martin, T., Tsarau, A., and Bihs, H., 2020. "A numerical framework for modelling the dynamics of open ocean aquaculture structures in viscous fluids". Appl. Ocean Res., p. 102410.

[7] Martin, T., and Bihs, H., 2021. "A non-linear implicit approach for modelling the dynamics of porous tensile structures interacting with fluids". J Fluids Struct, **100**, p. 103168.

[8] Martin, T., Kamath, A., and Bihs, H., 2020. "A Lagrangian approach for the coupled simulation of fixed net structures in a Eulerian fluid model". J Fluids Struct, **94**, p. 102962.

[9] Wang, G., Martin, T., Huang, L., and Bihs, H., 2020. "Numerical Simulation of Hydrodynamics Around Net Meshes Using REEF3D". In the ASME 2020 39th International Conference on Ocean, Offshore and Arctic Engineering. Volume 5: Ocean Space Utilization. Virtual, Online.. August 3–7, p. V005T05A002.

[10] Bihs, H., Kamath, A., Alagan Chella, M., Aggarwal, A., and Arntsen, Ø. A., 2016. "A new level set numerical wave tank with improved density interpolation for complex wave hydrodynamics". Comput Fluids, **140**, pp. 191–208.

[11] Osher, S., and Sethian, J. A., 1988. "Fronts propagating with curvature-dependent speed: Algorithms based on Hamilton-Jacobi formulations". J. Comput. Phys., **79**(1), pp. 12–49.

[12] Aggarwal, A., Pákozdi, C., Bihs, H., Myrhaug, D., and Alagan Chella, M., 2018. "Free Surface Reconstruction for Phase Accurate Irregular Wave Generation". J. Mar. Sci. Eng, **6**(3), p. 105.

[13] Jacobsen, N. G., Fuhrman, D. R., and Fredsøe, J., 2012. "A wave generation toolbox for the open-source CFD library: OpenFoam®". Int. J. Numer. Methods Fluids, **70**(9), pp. 1073–1088.

[14] Jiang, G.-S., and Shu, C.-W., 1996. "Efficient Implementation of Weighted ENO Schemes". J. Comput. Phys., **126**(1), pp. 202–228.

[15] Jiang, G.-S., and Peng, D., 2000. "Weighted ENO Schemes for Hamilton–Jacobi Equations". SIAM J. Sci. Comput., **21**(6), pp. 2126–2143.

[16] Shu, C.-W., and Osher, S., 1988. "Efficient implementation of essentially non-oscillatory shock-capturing schemes". J. Comput. Phys., **77**(2), pp. 439–471.

[17] Kristiansen, T., and Faltinsen, O. M., 2012. "Modelling of current loads on aquaculture net cages". J Fluids Struct, **34**, pp. 218–235.

[18] Chen, H., and Christensen, E. D., 2018. "Simulating the hydrodynamic response of a floater–net system in current and waves". J Fluids Struct, **79**, pp. 50–75.

[19] Gaeta, M. G., Segurini, G., Moreno, A. M., and Archetti, R., 2020. "Implementation and Validation of a Potential Model for a Moored Floating Cylinder under Waves". J. Mar. Sci. Eng, **8**(2), p. 131.

[20] Dong, S., You, X., and Hu, F., 2020. "Effects of wave forces on knotless polyethylene and chain-link wire netting panels for marine aquaculture cages". Ocean Eng., **207**, p. 107368.

[21] Fredriksson, D. W., Swift, M., Irish, J. D., Tsukrov, I., and Celikkol, B., 2003. "Fish cage and mooring system dynamics using physical and numerical models with field measurements". Aquac Eng, **27**(2), pp. 117–146.

[22] Huang, L., 2013. "Study on hydrodynamic characteristics of circular HDPE sea cage system with double floating tubes". PhD thesis, Ocean University of China.

[23] Hashiura, M., Hirabayashi, S., and Suzuki, H., 2016. "Experimental study of shape effect of floating body for vortex-induced motion". In 2016 Techno-Ocean (Techno-Ocean), pp. 74–79.